Photoinduced Architectural Transformation of Noncovalent Fluorescent Photochromic Organic Nanoparticles as Evidenced by Amplified Fluorescence Photoswitching

Thibault Gallavardin, Andrea Mulas, Lucie Norel, Stéphane Rigaut, Arnaud Brosseau, Rémi Métivier, Eléna Ishow

Photoinduced Architectural Transformation of Non-Covalent Fluorescent Photochromic Organic Nanoparticles Evidenced by Amplified Fluorescence Photoswitching

Thibault Gallavardin,[§,†] Andrea Mulas,[‡] Lucie Norel,[‡] Stéphane Rigaut,[‡] Arnaud Brosseau,[#] Rémi Métivier,[#] and Eléna Ishow[§]*

[§]Université de Nantes, CEISAM-UMR CNRS 6230, 2 rue de la Houssinière, 44 322 Nantes, France. [‡]Univ Rennes, CNRS, ISCR (Institut des Sciences Chimiques de Rennes) − UMR 6226, 35 000 Rennes, France. [#]Université Paris-Saclay, ENS Paris-Saclay, CNRS, PPSM, 91190 Gif-sur-Yvette, France.

KEYWORDS. Organic nanoparticles, fluorescence photoswitching, photochromism, amplification, dye self-sorting.

ABSTRACT. Dual nanoparticles endowed with emission photoswitching ability are produced by flash coprecipitation of fluorophores and photochromes into water in order to investigate the mutual interplay between the self-assembled photoactive units as a function of their respective ratio. Photophysical studies show that high fluorophore:photochrome ratios favor very fast on/off fluorescence photoswitching while the opposite is true for recovering emission thanks to the strong

antenna effects permitted by the spatially confined entities in nanoparticles. Attempts to regenerate the initial state upon visible irradiation reveal unexpected structural transformations, which results from the non-covalent dye self-assemblies. Morphological investigations support phototriggered photochrome clustering within and around the fluorescent core of the dual nanoparticles after a UV-vis cycle or irradiation, causing partition of the photoactive units. The photoinduced morphological changes open attractive prospects in the fabrication of smart drug delivery systems where active material release by external stimuli represents a very dynamic research area.

INTRODUCTION

Fluorescent organic nanoparticles (**FONs**), made out of small fluorophores or semi-conductive polymers, nowadays represent a remarkable part of the photoactive materials for bioimaging,[1,2] sensing[3] and tracking applications.[4,5,6] Their specific advantages reside in their molecular composition, devoid of any diluting matrix like silica or inert polymers, and their straightforward property modulation thanks to the versatile tools of organic synthesis.[7] Their particularly high payload of functional units gives rise to unexplored photophysical effects associated to the close packing of chromophores, which has been exploited to generate novel emission features through excimer[8] or exciplex formation,[9] and efficient energy transfer between energy-donating and accepting units.[10,11] This specific interest in **FONs** has much more recently been extended to another class of photoactive nanoparticles based on photochromic dyes.[12] Since most of photochromic reactions are accompanied with significant geometrical changes,[13] photoconversion within photochromic organic nanoparticles (**PONs**) can be dramatically impacted by structural confinement due to apparent restriction of the degrees of freedom.[14,15] Comparative studies between thin films, nanoparticles and solutions actually revealed accelerated conversions for nanoparticles as a result of cooperative interactions.[16,17] Since the vast majority of **FONs** and

PONs is fabricated through nanoprecipitation in water of concentrated solutions of hydrophobic dyes, hydration effects cannot be overlooked in the case of nanoparticles displaying significant interface with water. Nonlinear optical measurements of **FONs** comprising push-pull fluorophores evidenced interfacial dye organization at the nanoparticle surface[18] while studies in deuterated water showed increased fluorescence performances as a result of weakened vibrational coupling with water.[19] Other studies indicate that dyes with hydrogen bonding ability tend to form smaller nanoparticles as a result of higher solubility[20] while dye exchange between **FON** mixtures comprising amphiphilic dyes was revealed by investigating energy transfer phenomena.[21] This latter study was the first one to examine the composition evolution of organic nanoparticles in water. Several further works demonstrated the disintegration of organic nanoparticles in contact of hydrophobic biological membranes using dyes displaying solvatochromism in the excited state [22,23] or distance-dependent electron transfer properties.[24] All these transformations could be considered as a result of natural diffusion and interactions with the external media. However, photoinducing **FON** transformation would represent a further attractive step to generate stimuli-responsive nanomaterials with unexplored structural effects. In this context, pairing photochromes and fluorophores represents an attractive strategy to gain insight into the investigated transformation, the first photoactive molecules serving as actuators while the second ones would monitor the phototransformation. Such a combination has actually been explored with very buoyant interest since the seminal work of Irie et al,[25] that is currently expanded to fascinating systems to photoswitch or photomodulate the signal of devices in organic electronics,[26] and more recently address super-resolution microscopy issues.[27,28,29,30] Most investigations involved monodye nanoparticles where the photochromic and fluorescent units are covalently linked, thereby limiting straightforward performance modulation. With the progress toward bicomposite

nano-objects where dyes are merely self-assembled, novel questions are raised about the interactions developed, not only between the closely packed dyes, but also with their surroundings. Especially, mastering the architectural evolution and chemical composition of dual nanoparticles that are subjected to repeated photoirradiation steps and on/off fluorescence photoswitching due to the photoconversion of photochromes into emission quenchers, becomes of prime importance to achieve full reversibility and reproducibility. To address this issue, we report herein on the exploration of novel dual nanoparticles comprising specifically designed fluorophores and photochromes at various photochrome:fluorophore ratios. Comparative photophysical and photochromic investigations between blend and separated mixtures of nanoparticles are performed (Figure 1). They shine light on the optimal dye ratio requirements and main energy mechanisms in order to achieve amplified on/off fluorescence photoswitching in dual nanoparticles. The reported results offer new insights on the unexpected structural evolution of photoactivatable nanoparticles at the nanoscale, which could open stimulating prospects to design novel objects for on-command light-induced drug delivery.

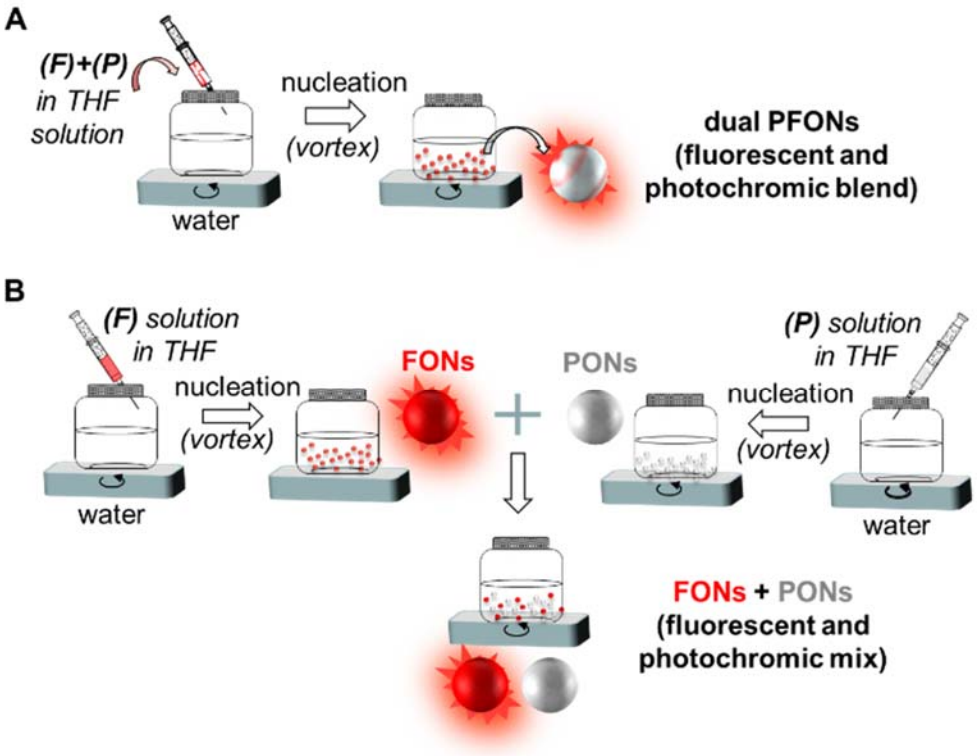

Figure 1. Schematic fabrication procedure: A) dual fluorescent and photochromic nanoparticles (**PFONs**) upon flash co-nanoprecipitation of **(F)** fluorophores and **(P)** photochromes, B) mix of fluorescent nanoparticles (**FONs**) and photochromic nanoparticles (**PONs**) upon separate flash nanoprecipitation and further combination of the dispersions.

METHODS

Fabrication of aqueous FON, PON and PFON dispersions

Spectroscopic grade THF, used for all preparations and photophysical studies, was purchased from Aldrich. **(F)** and **(P)** stock solutions in THF were prepared at a 2.4 mmol.L^{-1} concentration (resp. 2.0 and 1.6 wt. %). Pristine **FON** and **PON** dispersions were obtained by first diluting by half the stock solutions with THF and then quickly adding 50 µL of the resulting diluted solutions to a larger volume of Millipore® water (2.5 mL) under stirring. **PFONs** with varying **(F):(P)** molar

ratios (1:1, 2:1, 5:1) required the prior preparation of **F** and **P** mixtures at the right concentration. To this aim, a total volume of 100 μL of **(F)** and **(P)** dyes were prepared by adding to a fixed volume of 50 μL of **(F)** stock solution varied amounts of **(P)** stock solution, namely 50, 25, and 10 μL, and THF, namely 0, 25 and 40 μL to reach the targeted **(F):(P)** molar ratios, respectively 1:1, 2:1 and 5:1. Following the same protocol as that described for pristine **FON** and **PON** dispersions, 50 μL of the freshly above-prepared dye mixtures were added to 2.5 mL of Millipore® water to yield **PFON** dispersions.

Structural characterizations of organic nanoparticles

Dynamic light scattering (DLS). The hydrodynamic diameter and size dispersion of organic nanoparticles were determined by dynamic light scattering (DLS) by means of a nanoparticle size analyzer Cordouan (Vasco 3) equipped with a 40 mW diode laser operating at 658 nm. Measurements were collected in a backscattering mode at an angle of 135°. Measurements were carried out at 25 °C on aqueous solutions of nanoparticles. For each sample, intensity measurements were carried out in a multi-acquisition mode implying automatically adjusted correlograms, and averaged measurements on 6 acquisitions. Nanoparticle mean sizes and distribution widths were obtained by fitting each correlogram with a SBL algorithm, giving better description of multimodal distributions. Number representations of the size distribution were traced, assuming a refractive index value equal to 1.7 for organics, and extinction coefficient of 0.55 for UV-irradiated **PFONs**, which actually showed no significant incidence on the resulting mean diameter.

Zetametry. Measurements of ζ surface potential were carried out by means of a Zetasizer Nano ZS ZEN 3600 (Malvern). The samples were placed in disposable folded capillary cells (DTS1070).

Two sets of three measurements were realized for each sample and the zeta potential was calculated from electrophoretic mobility dispersion fitted by the Smoluchowski model.

Transmission electron microscopy. FON size measurements as dry samples were performed on diluted samples deposited on holey carbon-coated copper grids (300 mesh) purchased from Agar Scientific, and required the use of MO-Jeol 1230 microscope (80 kV).

Photophysical studies

Steady-state measurements. UV−visible absorption spectra were recorded using a Varian Cary 5E spectrophotometer. Emission spectra were recorded using a spectrofluorometer Fluorolog 3-Horiba mostly using $\lambda_{exc} = 450$ nm as the excitation wavelength that advantageously corresponded to minimal absorption of the (*c*)-(**P**) forms while being close to the (**F**) absorption maximum. Correction for the emission spectra with regard to the spectral response of the detector was automatically applied. Fluorescence quantum yields were determined in solution, referred to coumarin 540A in ethanol ($\Phi_f = 0.38$).

Time-resolved fluorescence measurements. Fluorescence time decays were measured in water or HBSS using the fully automated spectrofluorimeter (model Fluotime 300, PicoQuant) following the time-correlated single photon counting method. Excitation was performed using a pulsed laser diode (LDH-D-C-450B) working at 450 ± 10 nm with a 70 ps full width at half maximum. Fluorescence decays were recorded using a Hybrid-PMT detector combined with an acquisition temporal resolution up to 25 ps. A long-pass edged filter purchased from Semrock centered at 473 nm (BPL01-473R-25) was used to discard any possible contribution of excitation light scattering by the organic nanoparticle dispersions. Time fluorescence decay modeling was performed with EasyTau 1 software provided by Picoquant. All fluorescence intensity decays could be modeled after pulse reconvolution using a three-exponential law (1).

$$I(t) = \sum_{i=1}^{3} a_i \, exp(-t / \tau_i) \qquad (1)$$

with a_i count weight of the time constant τ_i. In order to take better into account the incidence of the energy transfer in the absence of collision within the organic nanoparticles, each time constant contribution was expressed as an amplitude fraction α_i defined as (2):

$$\alpha_i = \frac{a_i}{\sum_j a_j} \qquad (2)$$

The amplitude-averaged lifetime $< \tau_s >$ is then defined as (3):

$$< \tau_s > = \sum_{i=1}^{3} \alpha_i \tau_i \qquad (3)$$

Resonance energy transfer (FRET). The Förster radius R_0 can be estimated from the spectral overlap factor between the energy donor (**F**) and acceptor (**P**) (4).

$$R_0^6 = \frac{0.2108 \kappa^2 \Phi^\circ_D}{n^4} \int_0^\infty I_D(\lambda) \varepsilon_A(\lambda) \lambda^4 d\lambda \qquad (4)$$

with Φ°_D: fluorescence quantum yield of the donor in the absence of acceptor, n: refractive index of the solution, κ^2: orientation factor with $\kappa^2 = 0.476$ for dipoles in a rigid medium like self-assembled dyes within nanoparticles, I_D: emission intensity of the donor, ε_A: molar absorption coefficient of the acceptor.

Photochromic investigations

Steady-state measurements. Photochromic experiments were performed with solutions, magnetically stirred and placed in quartz cells, using a white light source Hg-Xe lamp (Hamamatsu

– LC8) equipped with single-band bandpass filters centered at 340 nm (22 nm fwmh), 488 nm (25 nm fwmh), or 540 nm (88 nm fwmh) purchased from Semrock. The absorption and emission spectra were recorded at various time intervals after irradiation using the spectrophotometer and spectrofluorometer respectively, described above. From ^{1}H NMR studies performed in the photostationary state (PSS), the photoconversion yield $\boldsymbol{\rho_{oc}^{P}}$ was assessed to be 92 % by comparative integration of the methyl proton signals. The photoconversion yield $\boldsymbol{\rho_{oc}^{NP}}$ for the *(o)→(c)* transformation of **PONs** and **PFONs** was assessed with regard to **(P)** in THF solution and **FON** absorption spectra, by using the formulae (5) and (6) to calculate the **(P)** contribution in **PFONs**, and taking advantage of exclusive absorption by **(F)** and **(P)** units at 480 and 597 nm respectively, for **PFONs** before UV irradiation.

$$\rho_{oc}^{NP} = \frac{A^{NP}(597)}{A^{cP}(604)} \times \frac{A^{oP}(340)}{\Delta A^{NP}(340)} \rho_{oc}^{P} \qquad (5)$$

$$\Delta A^{NP}(340) = A^{NP}(340) - A^{FON}(340) \times \frac{A^{NP}(480)}{A^{FON}(480)} \qquad (6)$$

where $A^X(\lambda)$ features the absorbance of species X (**PFON**, **FON**, closed and open **(P)** forms) at the wavelength λ, and $\boldsymbol{\rho_{oc}^{P}}$ the photoconversion yield of **(P)** in THF solution.

Photokinetic measurements. Time-resolved photoinduced cyclization and retrocyclization were recorded on magnetically-stirred (P) solutions in THF using as an excitation source a continuous Hg-Xe lamp (Hamamatsu – LC8). Irradiation was performed using the same single-band bandpass filters as those involved in steady-state measurements. The in-situ photodynamics of both reactions were followed by using a white light probe (Xenon 75 W) and a CCD-camera coupled with a spectrograph (Princeton Instruments). Irradiation powers were measured with a photometer (Ophir – Nova II) equipped with a photodiode (Ophir – PD 300 UV) in the UV (340 nm) at 0.18 mW.cm^{-2}

and in the visible range (547 nm) at 6.9 mW.cm^{-2}. Modeling and calculations of the *(o)→(c)* cyclization and *(c)→(o)* retrocyclization quantum yields, Φ_{oc} and Φ_{co} respectively, were performed only for **(P)** in THF solution at the absorption maximum wavelength (604 nm) of the *(c)* form where the *(o)* form does not absorb by means of an algorithm programmed by a home-made algorithm using Igor Pro software. The cyclization quantum yield Φ_{co} for **(P)** in THF solution upon irradiation at 340 nm was assessed to be equal to 0.69 while the retrocyclization quantum yield Φ_{co} upon irradiation at 540 nm was valued to be 1.3×10^{-2} (Table S2).

RESULTS AND DISCUSSION

Design and fabrication of pristine and dual fluorescent and photochromic nanoparticles

As depicted in Figure 1, photoactive organic nanoparticles are simply obtained from the quick addition into water of concentrated dye solutions prepared in a water-miscible solvent like tetrahydrofuran (THF). The main challenge upon working with non-doped functional nanoparticles lies in the retention, at least partly, of the photoactive properties of individual molecules in solution when going to self-assembled molecules in nanoparticles. One straightforward way relies on the introduction of bulky groups to create free volume and thus limit intermolecular π–π stacking that is deleterious for both emission and photochromism.[8] From our previous expertise, we focused our attention on the introduction of two *tert*-butyl substituted arms on a triarylamine core in the fluorescent units **(F)**, which helps maintain the fluorescence properties of the constituting molecules. Furthermore, these hydrophobic groups greatly contribute to the formation of well-dispersed and spherical nanoparticles in water as revealed by transmission electron microscopy (TEM) (Figure 2A). The triarylamine scaffold is completed with a charge

transfer structure that causes largely red-shifted emission, a pre-requisite for FRET photoswitching ruled by the spectral overlap between the fluorophore emission band and the absorption band of the closed forms of the photochrome. Since most of diarylethene compounds photocyclize into closed isomers absorbing around 600 nm, we introduced into the fluorophore backbone the benzothiadiazole unit known to impart large emission Stokes shift (Scheme S1).

As for the diarylethene derivative **(P)**, we chose the carboxylic derivative (Figure 2A, Scheme S2), displaying a rigid and elongated π-conjugated structure. Hence, dispersion interactions, namely π interactions, between **(P)** and the central charge-transfer backbone of the **(F)** units, supporting the radiative excited state (*vide infra*), should be favored within the bicomposite nanoparticles. Its acidic unit is expected to bring additional colloidal stability in water upon partial deprotonation of the dyes positioned at the water interface. Finally, the retained conjugated structure promotes the formation of closed form *(c)*-**(P)** with absorption depletion right in the area of maximum absorption of the **(F)** fluorophore (Figure 2B). Hence, selective excitation of the **(F)** units will be allowed in order to offer a rationale of the implied photophysical mechanisms for efficient on/off fluorescence photoswitching.

Comparative spectroscopic and photochromic properties between solutions and pristine nanoparticles

From spectroscopic measurements carried out on the fluorescent compound **(F)**, either in solution (toluene, THF) or as nanoparticle dispersions in water, we could notice three main features. Firstly, the absorption spectra display two intense bands, the first one in the UV range centred at around 339 nm that is hardly sensitive to the solvent polarity, and the second one in the

visible whose maximum absorption wavelength slightly varied from 466 to 459 nm when going from toluene to THF (Figure 2A). Such bands in the UV and visible range have been attributed by TDDFT computations to charge transfer from the triphenylamino core to respectively the benzothiadiazolyl moiety and the external biphenyl branches.[31]

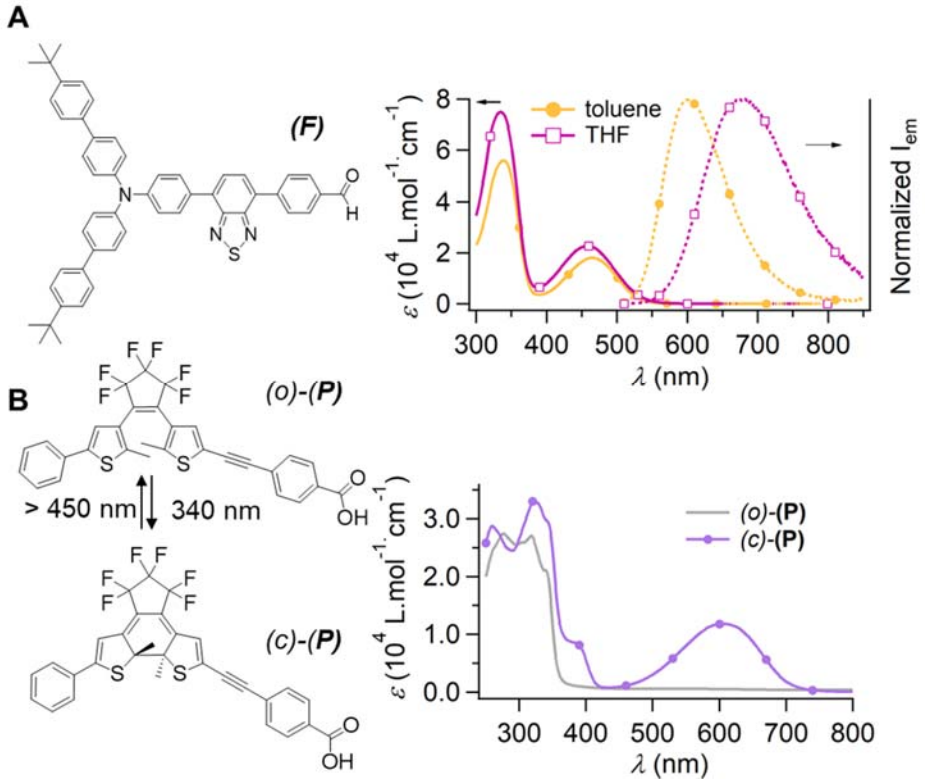

Figure 2. A) Structure and UV-vis absorption (bold line) and emission spectra (dotted line, λ_{exc} = 450 nm) of fluorophores **(F)** in toluene and THF solution. B) Structure and UV-vis absorption spectra of the *(o)* open and *(c)* closed isomers of photochrome **(P)** in THF.

Secondly, the fluorescence spectra show large dependence on solvent polarity with a band maximum shifting from 603 to 678 nm when going from toluene to THF and a Stokes shift varying from 4875 to 7037 cm^{-1}. These bathochromic and large Stokes shifts suggest substantial reorganization of the Franck-Condon excited state upon charge transfer, letting anticipate high

sensitivity to the molecular surroundings. Interestingly, the emission signal of **FONs** in water resembles that of THF solution, with a band maximum located at 654 nm (Figure 3A, Table S1). Its noticeable finer shape (fwhm = 2665 cm^{-1}) compared to that in THF solution (fwhm = 3200 cm^{-1}) could thus result from internal motions, more restricted for molecules self-assembled in nanoparticles compared to free-rotating molecules in solutions. Interestingly, this is in contrast with the absorption spectra that slightly broaden for **FON** dispersions compared to (**F**) one in solution. However, this observation may result from a distribution of dye geometries and additional interactions with the water molecules at the **FON** surface rather than from intermolecular interactions between the dyes. Indeed, no notable hypochromism of the charge transfer band in the visible, implying the triphenylamino and benzothiadiazolyl units, was observed when going from **(F)** in solution to (**F**) processed as **FONs** (Figure S1). Thirdly, whereas the fluorescence quantum yield Φ_f notably drops from 0.58 in toluene to 0.23 in THF solution for polarity reasons, its value remains very close between THF solution (Φ_f = 0.23) and nanoparticle dispersion in water (Φ_f = 0.27). Time-resolved fluorescence measurements follow the same trend with a monoexponential fluorescence decay at 5.86 ns in toluene that shortens to 4.08 ns in THF. All these features thus show the efficient role played by the bulky *tert*-butylphenyl groups to prevent fluorescence quenching upon fluorophore π–π stacking, thereby validating the adopted strategy.

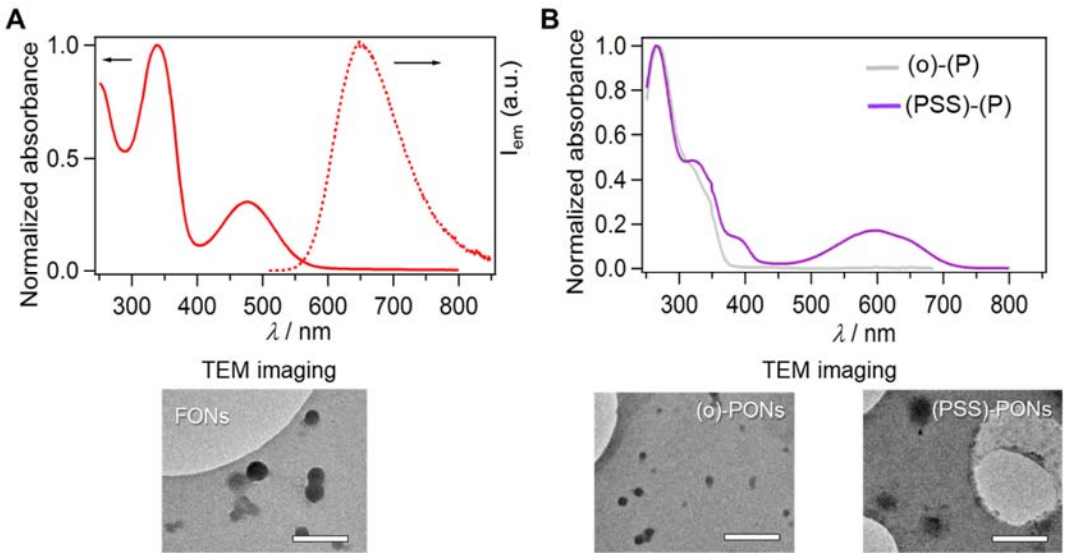

Figure 3. A) UV-vis absorption and emission spectra (λ_{exc} = 450 nm) of **FONs** in water and TEM imaging. B) UV-vis absorption of **PONs** in water with **(P)** photochromes in their open forms *(o)* and in the photostationary state *(PSS)* after irradiation at 340 nm, and TEM imaging. Scale bar: 100 nm.

Given the quite large similarity between THF and water in terms of photophysics for **(F)** and **FONs** respectively, all spectroscopic and photochromic analyses of photochromes **(P)** in solution were conducted in THF solution. The absorption spectra of the open *(o)*-**(P)** form in THF and **PONs** in water show quite distinct energy profiles contrarily to the closed *(c)*-**(P)** forms, appearing similar (Figure 2B, Figure 3B, Table S2). For **(P)** in THF solution, two intense bands in the UV at around 270 and 320 nm were observed before irradiation, the latter appearing as a shoulder for **PONs**. Photocyclization, performed at 340 nm, yielded an intense purple solution due to a novel absorption band characteristic of the **(P)** closed forms, centered at 604 nm in THF solution and 597 nm for aqueous **PON** dispersions (Figure S2-S3). Full reversibility upon irradiation at 540 nm of **(P)** solution in its PSS was obtained as the initial absorption spectrum of the open form was restored (Figure S2B). By contrast, for aqueous **PON** dispersions, reversibility was not fully

achieved (Figure S3C). Since dye degradation cannot be evoked from experiments in solution, we will see later another possible explanation to support this interesting observation. The absorption spectra deserve additional important comments. The visible band at the photostationary state appears more structured and less intense for **PONs** than for **(P)** solution, despite similar initial absorbance. The lower photoconversion yield ($\boldsymbol{\rho_{oc}^{PON}}$= 0.66 against 0.92 for **(P)** in THF solution) and the structured absorption band for **PONs** let us suggest non negligible intermolecular π−π interactions within the nanoparticles that would partly impede molecular geometry change upon photoirradiation. Finally, one can notice that the band in the visible range strongly overlaps with the emission band of **(F)** or **FONs**, as required for efficient fluorescence photoswitching upon photoinduced energy transfer. Using random dipole orientation in a rigid medium (orientation factor κ^2 = 0.476) and considering the emission spectra of **FONs** in water and absorption spectra of **(P)** in THF solution (rather than that of PON where dye interactions operate), the Förster radius R_0, featuring the distance at which the probabilities for the fluorophores to deactivate in the absence of quencher or to undergo energy transfer are equal, was calculated to be 3.4 nm. All these data let us anticipate significant electronic interplay between fluorophores **(F)** and photochromes **(P)**, once they are tightly confined in dual nanoparticles.

Tuning fluorescence photoswitching in dual nanoparticles

We thus generated dual organic nanoparticles **PFONs**, using the same protocol as that described above for pristine **FONs** and **PONs**. To apprehend their fluorescence photoswitching capability upon energy transfer, we varied the molar **(F)**:**(P)** ratio (1:1, 2:1, 5:1), starting from an equimolar ratio and ending up with a fivefold default of the photochromic units compared to the fluorescent ones. To make the measurements comparable, all **PFONs** were fabricated using THF solutions containing similar amounts of fluorophores. The solutions were adjusted to the same volume by

adding THF complements, so that solutions with identical concentrations in fluorophores were precipitated each time into water. The resulting absorption spectra show one intense band in the UV range, characteristic of overlapping **(P)** and **(F)** contributions, and one less intense band in the visible range, typical of **(F)** units as long as **(P)** units remain in their open form (Figure 4A).

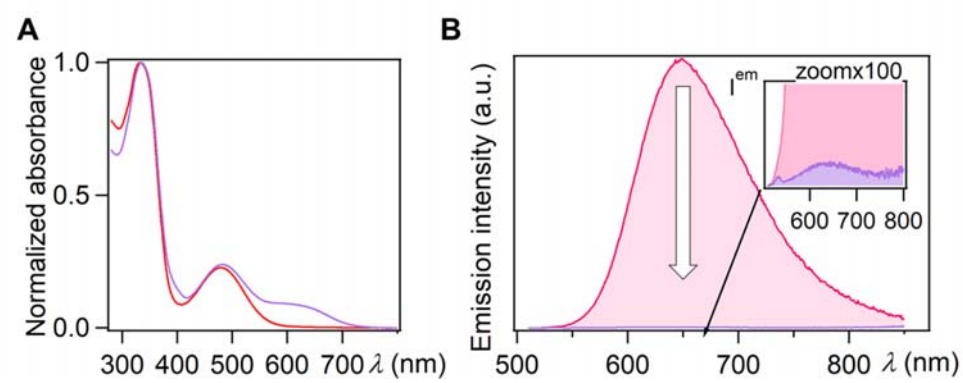

Figure 4. Evolution of the absorption and emission spectra (λ_{exc} = 450 nm) of **1:1 PFONs** in water before (red) and after (purple) irradiation at 340 nm (50 mW.cm^{-2}, 10 s irradiation) under stirring. The white tail figures the dramatic decrease in emission.

All fabricated **PFONs** show identical emission maximum wavelengths λ_{max}^{em} at 648 nm, coming from the **(F)** units (Table S3), while Φ_f dropped to 0.11-0.13 for **PFONs**. The hypsochromic absorption shift and emission intensity decrease observed for **PFONs** already suggest quite tight **(F)** and **(P)** dye interactions and intermixing thereof.

After irradiation at 340 nm under the same conditions as those used for pristine **PONs**, a new absorption band centered at 630 nm arose following the formation of the (**P**) closed forms. Unexpectedly, its final absorbance at the PSS did not show direct correlation with the initial (**P**) stock solution concentration, again evoking particular intermolecular interactions in the solid state. At this stage, we can discard any difference in light penetration in the nanoparticles due to distinct (**F**):(**P**) ratios since all absorption photokinetic rate constants $k^{UV}(abs^{630})$ were found to be the same

(Figure 5A, Table S3). Irradiation at 340 nm also caused quenching of the **PFON** emission whose FRET efficiency clearly depends on the (**F**):(**P**) ratio, but no longer in a linear manner. The emission signal remarkably declined by 82.7 % of the initial value for a 5:1 ratio, and eventually by 98.9 and 99.7 % for 2:1 and 1:1 ratios respectively (Figure 4B and Figure S**4**-S**6**). Such emission decrease directly corresponds to the energy transfer efficiency Φ_{ET} since the absorbance at the excitation wavelength remained constant (Table S3). Remarkably, not only the emission residue but also the emission decrease rate are function of the (**P**) amount within the nanoparticles. Indeed, for 1:1 **PFONs**, accumulation of enough closed forms required hardly less than 10 s to induce almost complete quenching through energy transfer, against 60s and partial quenching for **5:1 PFONs** (Figure 4, Figure 5B). Very interestingly, two features could be noticed. First, upon UV irradiation, the drop of emission quenching is far faster than the absorbance rise at 630 nm ($k^{UV}(em^{530}) > k^{UV}(abs^{630})$, characteristic of the formation of (**P**) closed isomers (Figure 5A and 5B, Table S3). Secondly, the photokinetic rate constant $k^{UV}(em^{650})$ of the emission quenching increases with the amount of coprecipitated diarylethenes relative to (**F**) one. By contrast, the rate constant of (**P**) photocyclization, characterized by the absorbance rise at 630 nm, was found to be quite the same whatever the amount of coprecipitated (**P**) photochromes, which means that the generation of the (**P**) closed forms is not impeded by the presence of the (**F**) fluorophores (Table S3).

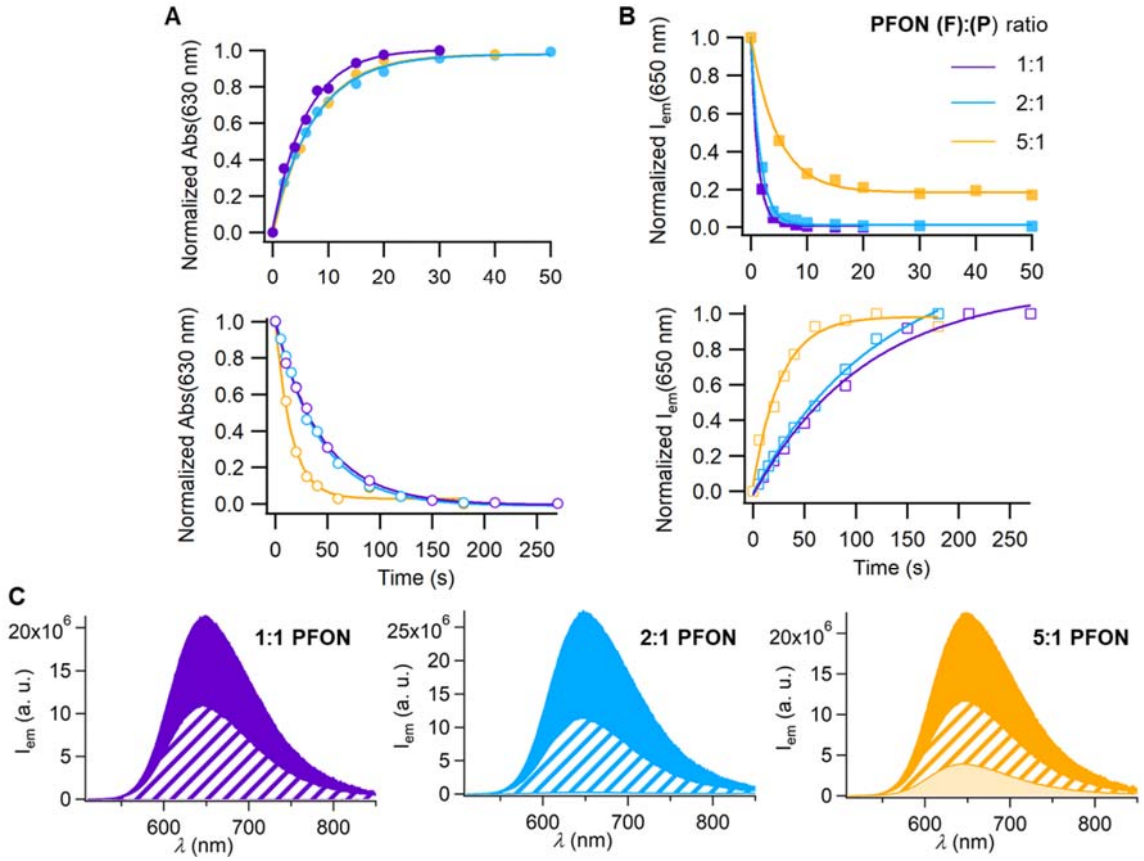

Figure 5. Normalized spectral evolution of aqueous dispersions of **PFONs** with **(F):(P)** ratios varying according to 1:1, 2:1 and 5:1 under irradiation at 340 nm (plain symbols) and 488 nm (empty symbols): A) Change in the normalized absorbance at 630 nm (round), B) Change in the normalized emission at 650 nm (λ_{exc} = 450 nm) (square), C) Change in the emission spectra before UV irradiation (plain down to the baseline), after UV irradiation at 340 nm (clear tint only visible for a 5:1 ratio) followed by irradiation at 488 nm (hatched area). Irradiation powers at 340 and 488 nm were fixed at 50 mW.cm^{-2}.

The faster emission evolution compared to the absorbance rise of the closed forms can be ascribed to cooperative energy transfer by the surrounded closed forms, thereby amplifying the fluorescence photoquenching effect, as previously proposed for nanoparticles made out of diarylethenes

covalently linked to fluorophores.[12] Interestingly, a relatively slower decrease rate for the emission signal is encountered in our case but turns to be larger than that reported for the sole example to our knowledge of non-covalently linked photoactive dyes in non-polymeric nanoparticles.[32] Evoking distinct Förster radii R_0 is actually insufficient to explain such difference since **PFONs** in our case display the smaller value. Energy migration through hopping, promoted by extended π–π aggregation of fluorophores and photochromes and more generally conjugated organic dyes[33] confined within nanoparticles, could reasonably be evoked as an additional mechanism underpinning the on/off switching efficiency. This would require substantial calculations to apprehend the spatial delocalization of excitons as reported for π-conjugated molecular materials,[34,35] which is beyond the scope of the reported studies.[36,37] Nevertheless, to support such assumption, we noticed that **FONs** precipitated in deuterated water, displayed enhanced amplitude-averaged lifetime $<\tau_s>$ = 3.75 ns compared to 2.77 ns. Since vibrational coupling mediated by hydrogen bonds can induce radiationless deactivation of polar excited states, change in the global emission of hydrophobic organic nanoparticles expelling water molecules could be ascribed to the occurrence of energy migration from the surface until the core thanks to extensive molecular orbital overlap between the self-assembled fluorophores.[19]

In order to apprehend the reversibility of the emission photoswitching process, irradiation in the visible at 540 nm where the closed **(P)** forms absorb was performed. As reported for pristine **PONs**, cycloreversion could efficiently be achieved. Using this wavelength could appear logical at the first sight but makes the photoconversion analyses less straightforward as the number of absorbed photons changes over time due to the transformation of the *(c)*-**(P)** forms into the *(o)*-**(P)** ones. We thus exploited the ability of **(F)** fluorophores to cause efficient FRET within the dual nanoparticles by irradiating at 488 nm where **(F)** units exclusively absorb, hence absorbance at the irradiation

wavelength remains constant. Full reversibility for all **PFON** compositions was achieved as the absorption band above 600 nm and characteristic of *(c)*-(**P**) completely vanished while the initial absorption spectra before UV irradiation were restored (Figure S7). Plotting normalized absorbance (Figure 5A) and emission evolutions (Figure 5B) as a function of the irradiation time yields very distinct dynamics between the closure and opening processes, characterized by the rate constants $k^{VIS}(em^{650})$ in emission, and $k^{VIS}(abs^{630})$ in absorption.

Here, the absorption band at 630 nm of the closed **(P)** forms readily disappeared, but the decrease rate $k^{VIS}(abs^{630})$ differed between the compositions. Nanoparticles containing less photochromes, like **5:1 PFONs**, revert back to the **(P)** colorless forms much faster (Table S3). Hence, the accelerated photokinetic effects in absorption and emission observed with higher **(F):(P)** ratios readily support the aforementioned assumption of FRET mechanism, completed by possible additional energy migration, responsible for *(c)*-**(P)** opening. Here, larger amounts of **(F)** units foster enhanced antenna effects to the closed **(P)** forms in the same way as larger amounts of open **(P)** forms lead to faster fluorescence extinction. In our case, heating effects as recently reported in an interesting study, showing photothermal effects at the nanoscale as a possible reason of the amplified cycloreversion step of diarylethene nanoparticles, can be ruled out to much a two low fluence and continuous irradiation regime used in our conditions.[38] So, to sum up the reported photokinetics, the faster quenching of the emission intensity with regard to the rate of (*o*)→(*c*)-(**P**) transformation results from the probability of one diarylethene in its closed form to quench a multifold of vicinal fluorophores, which cannot be achieved in solution. Such nonlinear behavior can also be noted with the (*c*)→(*o*)-(**P**) retrocyclization, photosensitized by fluorophores (**F**). The larger the amount of fluorescent units with respect to the (*c*)-(**P**) ones, the faster the retrocyclization

rate due to a higher probability of transferring the energy from (**F**) to promote reopening of the diarylethenes.

Finally, the last unexpected feature relies on the much slower and uncomplete recovery of the emission signal compared to the decrease of the absorption band at 630 nm. All compositions provide similar values for the emission signal recovery, representing half of the initial intensity before UV irradiation (Figure 5C). Such unexpected results prompted us to perform cyclic experiments, namely successive UV-vis irradiation steps to understand the underlying phenomena. For questions of sensitivity, we restricted our studies to the **1:1 PFON** composition. Ten cycles were thus applied (Figure 6). A continuous decrease in the emission signal was observed after each cycle, the loss in intensity being maximal after the first irradiation cycle. Conversely, absorbance at 630 nm related to the closed photochromes remains almost constant before starting to slowly decline. These observations offer strong discrepancy with the reversible absorbance and emission recoveries reported for photochromes and fluorophores covalently linked, either directly[39] or through polymer chains[40,41] within nanoparticles. We first explored the possibility of fluorophore photobleaching upon irradiation to explain the notable loss of emission after one UV-visible irradiation cycle. While visible irradiation had no impact, prolonged UV irradiation over 60 s only generated a 13 % decrease in the emission signal at 650 nm, which rules out photodegradation of **(F)** units as the main reason of the absence of **PFON** emission recovery.

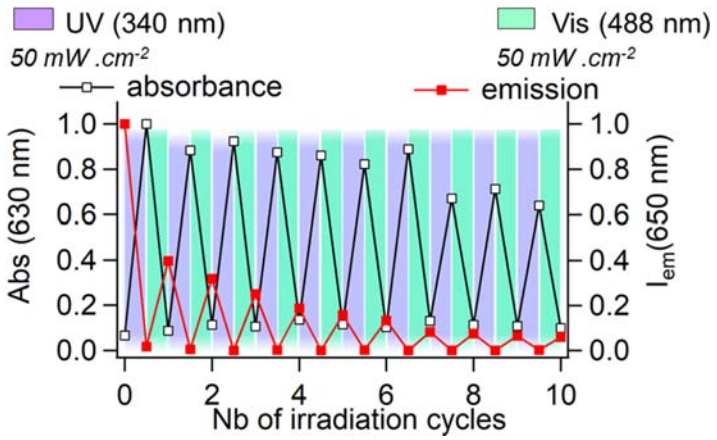

Figure 6. Evolution of the absorbance at 630 nm and emission intensity signal at 650 nm (λ_{exc} = 450 nm) of **1:1 PFONs** in water upon ten successive UV-visible irradiation cycles (alternative irradiations at 340 nm (50 mW.cm^{-2} – 20 s duration) and 488 nm (50 mW.cm^{-2} – 250 s duration).

Phototriggered dye segregation within nanoparticles

To go a step further in the understanding of the limited emission reversibility, we examined the microscopic fate of the photoirradiated **1:1 PFONs** by performing TEM and DLS analyses. Before irradiation, TEM imaging revealed well-defined and spherical nanoparticles that tend to spread after UV irradiation not only for **PONs** (Figure S8) but also for **1:1 PFONs** (Figure 7B), as if the photochromic dyes were leaking out. After subsequent irradiation in the visible range at 540 nm, the nanoparticles did not recover their initial shape but nevertheless appeared more delineated than after UV irradiation. The blurry shape of the UV-irradiated nanoparticles makes the determination of size distribution too unprecise, which prompted us to correlate TEM analyses with DLS measurements. The latter revealed slight shrinkage of **1:1 PFONs** after UV irradiation, which appeared more clearly on the number-weighted size distribution. (Figure 7C and Table S4).

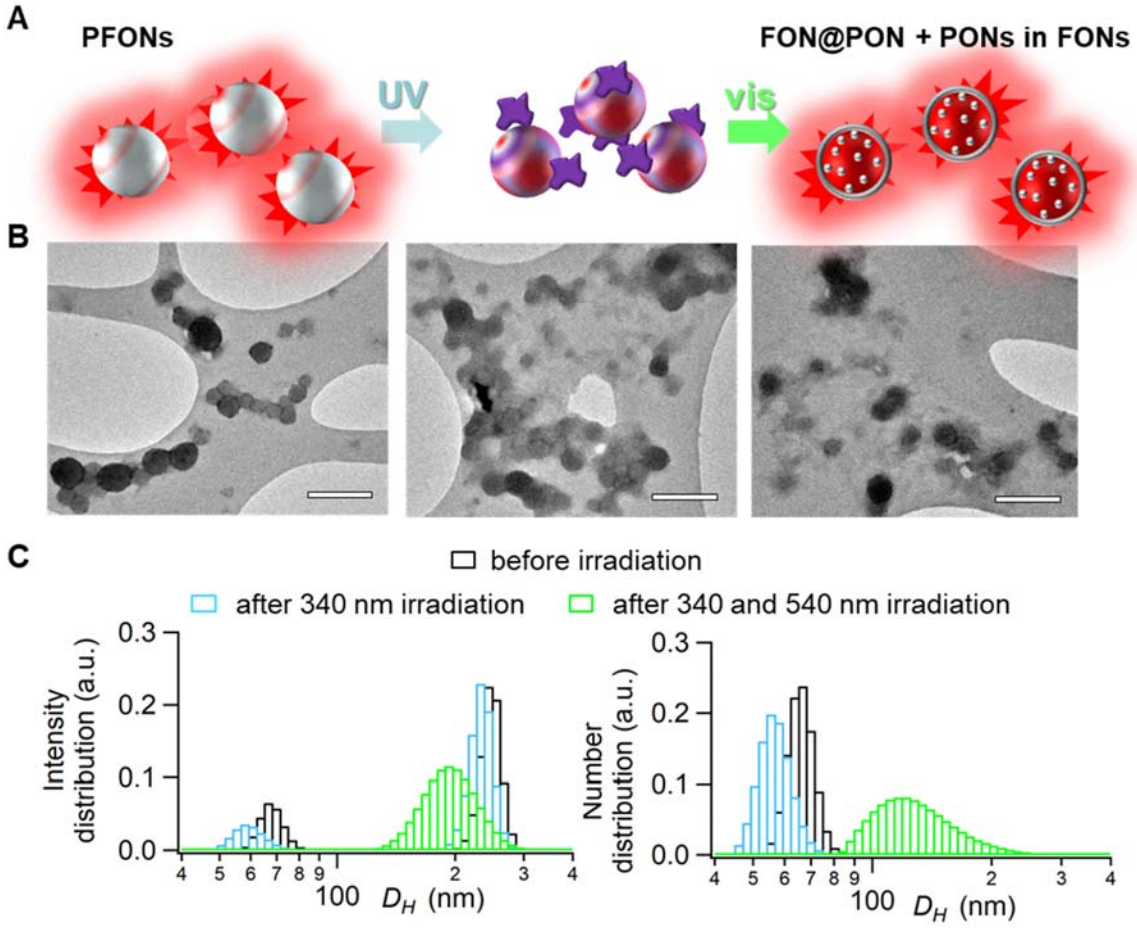

Figure 7. A) Schematic evolution, B) TEM imaging (scale bar 200 nm), and C) Intensity-weighted and number-weighted size distributions obtained by DLS measurements of **1:1 PFONs** in water, before irradiation, after UV irradiation (340 nm), and after a UV-vis irradiation cycle (340 and then 540 nm).

The most remarkable feature relies on the size distribution after ulterior irradiation at 540 nm where the size distribution considerably broadens (Figure 7C). These geometrical changes were also accompanied by a large modification of the zeta potential ζ measured at-21.9 ± 3.4 mV before UV irradiation and -22.9 ± 3.6 mV after UV irradiation, and evolving to -32.1 ± 3.7 mV after additional irradiation at 540 nm. The latter value turns to be comparable to those of pristine **FONs**

(-34.0 ± 4.4 mV) and **PONs** (-31.0 ± 3.6 mV). All these observations indicate large structural changes after one UV-vis irradiation cycle that may be caused by (**P**) diffusion within the nanoparticle up to the surface. Due to the large hydrophobic character of (**P**) dyes in their open and closed forms, extensive dissolution of (**P**) in water appears largely unfavorable as already investigated with aromatic fluorophores comprising acidic units and amenable to efficient self-assembling in water.[20] The fact that repetitive UV-vis cycling is accompanied with a steadily decreasing absorbance of the (*c*)-(**P**) form suggests less efficient (*o*)→(*c*) photoconversion, which may reflect (**P**) clustering inside and right at the periphery of **FON**s.

To examine the assumption of **(P)** clustering and segregation, we investigated the photophysical properties of a **PON+FON** mixture, by adding together separately prepared **PON** and **FON** dispersions, following an equimolar ratio in **(P)** and **(F)** dyes. To our surprise, a significant emission decrease at 650 nm occurred after UV illumination, leading to an energy transfer efficiency of 73.0 % against 99.7 % for **1:1 PFONs** (Figure S9) and a photoconversion yield of 72 %, close to that found for **PONs** and significantly larger than those for all **PFONs** (Table S3). Moreover, only half of the initial emission intensity for the **PON+FON** mixture was recovered after a photoinduced closure-opening cycle, which recalls previous observations with **PFON** dispersions, whatever the **(F):(P)** molar ratio (Figure S4-S6). Such unexpected results tend again to suggest non-negligible interactions between both kinds of nanoparticles, mediated through the hydrophobic backbones of their dye units. Dye co-precipitation to form pure **FONs** and **PONs** instead of dual **PFONs** could thus reasonably be questioned. It turns out that the decrease rates $k^{VIS}(abs^{630})$ in the *(c)*-**(P)** absorbance upon visible irradiation were found notably faster (3 to 8 times higher) for **PFONs** compared to that for the **PON+FON** mixture (Table S3). Since retrocyclization is here assisted by energy transfer or migration, physically close **(F)** and **(P)** units

favor more efficient retrocyclization, hence tight intermixing of **(F)** and **(P)** within **PFONs** can reasonably be envisaged. Such spatial vicinity seems to be essential to observe on/off fluorescence photoswitching since an equimolar solution of (**F**) and (**P**) in THF showed no significant change in the (**F**) emission intensity upon UV phototransformation of (**P**) into its colored form (Figure S10). It is worth noting the higher absorbance of the closed form at 597 nm, in agreement with the absence of geometrical constraints in solution compared to nanoparticles. To support further the assumption of dye co-precipitation within the same nanoparticle, time-resolved fluorescence measurements were performed by exciting at 450 nm and detecting the intensity decay at 650 nm. After UV irradiation, the amplitude-averaged lifetime $<\tau_s>$ for the **PON+FON** mixture was actually calculated to be around 1.95 ns, close to 2.24 ns for **FONs** (Figure S11, Table S5). On the contrary, **1:1 PFON** dispersions displayed a significantly shorter value for $<\tau_s>$ at 0.89 ns. Such a fluorescence decay shortening and the fact that the most efficient UV-photoswitching process was observed in **PFONs** comprising a high number of **(P)** units, let us propose that only vicinal photochromic and fluorescent units can produce a notable decrease in the emission decay and intensity signal.

Based on TEM images and all photophysical investigations, we thus propose a tentative schematic explanation for the absence of full emission recovery noticed for all **PFONs**. After one UV-vis irradiation cycle, **PFONs** are likely to evolve toward the formation of **FONs** doped with very small **PONs**, and possibly additionally coated with small **PONs**, similar to what could happen for the **PON+FON** mixture where **PONs** can only interact with the **FON** surface. Such an architectural evolution would be highly favored by π–π interactions between the aromatic structure of (**P**) (especially in its close form), and the hydrophobic character of (**F**) units and **FONs**. It would support the decreasing absorption of the closed (**P**) forms upon UV-vis cycling as a result of more

geometrically hampered (**P**) in small **PONs**. In the same way, the steadily decrease in the fluorescence signal is likely to mainly result from changes in the local surroundings of the fluorophores. We already noticed a lower emission quantum yield when (**F**) were mixed with (**P**) within **1:1 PFON** (Φ_f = 0.11) compared to the situation of pure **FONs** (Φ_f = 0.27) (Table S1). Such quenching was also observed for mixed **PON** and **FON** dispersions in a 1:1 ratio (Φ_f = 0.17). By contrast, the averaged fluorescence decays of **1:1 PFON** and **PON+FON** dispersions were much less impacted, with only a 15 and 4 % reduction respectively compared to that of **FONs** (Table S1, Figure S11). This suggests that (**P**) in its open form can exert deleterious hydrogen bonds and strong π–π interactions with the (**F**) units, leading to non-fluorescent adducts in their ground state. The strong reduction of the fluorescence intensity undergone after the first UV-vis cycle is of particularly interest and thus tends to evoke extensive (**P**) reorganization and segregation thereof, until reaching a plateau. Following all these observations, the generation of numerous tiny **(P)** clusters in close contact with (**F**) and leading to fluorescence quenching in the ground state could appear as a quite plausible explanation for the lack of on/off emission photoswitching and the resulting emission intensity reduction. Whereas previous studies have evidenced composition evolution of amphiphilic FONs over time due to interparticle molecular exchange,[21] this is the first time to our knowledge that photoinduced segregation within functional organic nanoparticles is reported, pointing out the need for long-term composition follow-up.

CONCLUSIONS

To conclude, these studies describe the ubiquitous non-covalent association of fluorophores and diarylethene derivatives to form upon flash nanoprecipitation photoswitchable fluorescent organic

nanoparticles with varying ratios of fluorophores and photochromes. Photokinetics in emission and absorption confirm the FRET mechanism operating between the fluorophores and photochromic units to induce accelerated fluorescence photoswitching of the resulting nanoparticles. They remarkably point out the fact that fine compromise regarding the respective amounts of fluorophores and photochromes needs to be found to achieve high speed and large on-off fluorescence photoswitching efficiency induced for both UV-assisted cyclization and visible-assisted retrocyclization. Very interestingly, segregation of dyes, initially randomly spread within organic nanoparticles, could be phototriggered, presumably due to the large change in hydrophobicity and hydrophilicity undergone by the closed forms of the photochromic units, diffusing inside and outside the core of the dual nanoparticles. Photochrome clustering into small nanoparticles, either dispersed in **FONs** or coating the **FON** surface, is evoked to explain the unexpected absorbance and emission photoswitching evolution upon UV-vis cycling. Such novel results emphasize the tight interactions established not only between the space-confined aromatic dyes but also between distinct organic nanoparticles in high concentration, promoting significant energy migration in addition to the usually evoked FRET mechanism. In some respect, such results demonstrate that organic nanoparticles, comprising small π-conjugated molecules, actually behave like P-dots where the self-assembled semiconducting polymers support efficient exciton migration and long-distance sensing.[42,43] To our knowledge, this is the first time that phototriggered self-sorting of dyes within small-molecule based organic nanoparticles is reported. These results open promising perspectives in the field of nanomedicines where smart photoactivatable drug nanocarriers represent a stimulating area of research.

ASSOCIATED CONTENT

Supporting Information. Synthesis procedures for fluorophore (F) and photochrome (P), photoswitching experiments involving absorption and emission spectra as well as time-resolved fluorescence measurements, TEM images of dual nanoparticles.

AUTHOR INFORMATION

Corresponding Author

* elena.ishow@univ-nantes.fr.

Present Addresses

†Université de Rouen, UMR-CNRS 6014 COBRA, 1 rue Tesnière, 76 821 Mont Saint Aignan, France.

Author Contributions

The manuscript was written through contributions of all authors. All authors have given approval to the final version of the manuscript.

ACKNOWLEDGMENT

We acknowledge B. Bouchet and L. Lartigue for access to Nantes-Angers INRAE BIBS platform for TEM measurements. We are very grateful toward CNRS and Région Bretagne for funding the "Rennes-Nantes Materials" programme ("NAMID" and "SAD Redoxlux" projects), allowing for Dr. A. Mulas's recruitment, and the French National Agency for funding the ANR-12-BS07-0010-01 programme ("RuOxLux" project) allowing for Dr. T. Gallardin's recruitment.

REFERENCES

(1) Mei, J.; Huang, Y.; Tian, H. Progress and Trends in AIE-Based Bioprobes: A Brief Overview. *ACS Appl. Mater. Interfaces* **2018**, *10*, 12217-12261.

(2) Liu, B.; Tang, B. Z. Aggregation-Induced Emission: More Is Different. *Angew. Chem. Int. Ed.* **2020**, *59*, 9788-9789.

(3) Gao, M.; Tang, B. Z. Fluorescent Sensors Based on Aggregation-Induced Emission: Recent Advances and Perspectives. *ACS Sensors* **2017**, *2*, 1382-1399.

(4) Kaeser, A.; Schenning, A. P. H. J. Fluorescent Nanoparticles Based on Self-Assembled pi-Conjugated Systems. *Adv. Mater.* **2010**, *22*, 2985-2997.

(5) Wu, C.; Chiu, D. T. Highly Fluorescent Semiconducting Polymer Dots for Biology and Medicine. *Angew. Chem. Int. Ed.* **2013**, *52*, 3086-3109.

(6) Fery-Forgues, S. Fluorescent Organic Nanocrystals and Non-doped Particles for Biological Applications. *Nanoscale* **2013**, *51*, 8428-8437.

(7) Biesen, L.; Nirmalananthan-Budau, N.; Hoffmann, K.; Resch-Genger, U.; Müller, T. J. J. Solid-State Emissive Aroyl-S,N-Ketene Acetals with Tunable Aggregation-Induced Emission Characteristics. *Angew. Chem. Int. Ed.* **2020**, *59*, 10037-10041.

(8) Ochi, J.; Tanaka, K.; Chujo, Y. Recent Progress in the Development of Solid-State Luminescent o-Carboranes with Stimuli Responsivity. *Angew. Chem. Int. Ed.* **2020**, *59*, 9841-9855.

(9) Hestand, N. J.; Spano, F. C. Expanded Theory of H- and J-Molecular Aggregates: The Effects of Vibronic Coupling and Intermolecular Charge Transfer. *Chem. Rev.* **2018**, *118*, 7069-7163.

(10) Campioli, E.; Rouxel, C.; Campanini, M.; Nasi, L.; Blanchard-Desce, M.; Terenziani, F. Enforcing Luminescence at Organic Nanointerfaces: Luminescence Spatial Confinement and Amplification in Molecular-Based Core–Shell Nanoparticles. *Small* **2013**, *9*, 1982-1988.

(11) Hoang, S.; S. Olivier; Cuenot, S.; Montillet, A.; Bellettre, J.; Ishow, E. Microfluidic Assisted Flash Precipitation of Photocrosslinkable Fluorescent Organic Nanoparticles for Fine Size Tuning and Enhanced Photoinduced Processes. *ChemPhysChem* **2020**, *21*, 2502-2515.

(12) Fukaminato, T.; Ishida, S.; Metivier, R. Photochromic Fluorophores At The Molecular And Nanoparticle Levels: Fundamentals And Applications Of Diarylethenes. *NPG Asia Mater.* **2018**, *10*, 859-881.

(13) Boelke, J.; Hecht, S. Designing Molecular Photoswitches for Soft Materials Applications. *Adv. Opt. Mater.* **2019**, *7*, 1900404.

(14) Métivier, R.; Badré, S.; Méallet-Renault, R.; Yu, P.; Pansu, R. B.; Nakatani, K. Fluorescence Photoswitching in Polymer Matrix: Mutual Influence between Photochromic and Fluorescent Molecules by Energy Transfer Processes. *J. Phys. Chem. C* **2009**, *113*, 11916–11926.

(15) Fukaminato, T.; Umemoto, T.; Iwata, Y.; Yokojima, S.; Yoneyama, M.; Nakamura, S.; Irie, M. Photochromism of Diarylethene Single Molecules in Polymer Matrices. *J. Am. Chem. Soc.* **2007**, *129*, 5932-5938.

(16) Spangenberg, A.; Metivier, R.; Gonzalez, J.; Nakatani, K.; Yu, P.; Giraud, M.; Leaustic, A.; Guillot, R.; Uwada, T.; Asahi, T. Multiscale Approach of Photochromism: Synthesis and Photochromic Properties of a Diarylethene in Solution, in Nanoparticles, and in Bulk Crystals. *Adv. Mater.* **2009**, *21*, 309-313.

(17) Snell, K. E.; Mevellec, J.-Y.; Humbert, B.; Lagugné-Labarthet, F.; Ishow, E. Photochromic Organic Nanoparticles as Innovative Platforms for Plasmonic Nanoassemblies. *ACS Appl. Mater. Int.* **2015**, *7*, 1932-1942.

(18) Daniel, J.; Bondu, F.; Adamietz, F.; Blanchard-Desce, M.; Rodriguez, V. Interfacial Organization in Dipolar Dyes-based Organic Nanoparticles probed by Second-Harmonic Scattering. *ACS Photonics* **2015**, *2*, 1209-1216.

(19) Boucard, J.; Linot, C.; Blondy, T.; Nedellec, S.; Hulin, P.; Blanquart, C.; Lartigue, L.; Ishow, E. Small Molecule-Based Fluorescent Organic Nanoassemblies with Strong Hydrogen Bonding Networks for Fine Tuning and Monitoring Drug Delivery in Cancer Cells. *Small* **2018**, *14*, 1802307.

(20) Faucon, A.; Lenk, R.; Hemez, J.; Gautron, E.; Jacquemin, D.; Le Questel, J.-Y.; Graton, J.; Brosseau, A.; Ishow, E. Fluorescent Carboxylic and Phosphonic Acids: Comparative Photophysics from Solution to Organic Nanoparticles. *Phys. Chem. Chem. Phys.* **2013**, *15*, 12748-12756.

(21) Kaeser, A.; Fischer, I.; Abbel, R.; Besenius, P.; Dasgupta, D.; Gillisen, M. A. J.; Portale, G.; Stevens, A. L.; Herz, L. M.; Schenning, A. Side Chains Control Dynamics and Self-Sorting in Fluorescent Organic Nanoparticles. *ACS Nano* **2013**, *7*, 408-416.

(22) Faucon, A.; Benhelli-Mokrani, H.; Córdova, L. A.; Brulin, B.; Heymann, D.; Hulin, P.; Nedellec, S.; Ishow, E. Are Fluorescent Organic Nanoparticles Relevant Tools for Tracking Cancer Cells or Macrophages? *Adv. Healthcare Mater.* **2015**, *4*, 2727-2734.

(23) Ishow, E.; Brosseau, A.; Clavier, G.; Nakatani, K.; Tauc, P.; Fiorini-Debuisschert, C.; Neveu, S.; Sandre, O.; Leaustic, A. Multicolor Emission of Small Molecule-Based Amorphous Thin Films and Nanoparticles with a Single Excitation Wavelength. *Chem. Mater.* **2008**, *20*, 6597-6599.

(24) Boucard, J.; Briolay, T.; Blondy, T.; Boujtita, M.; Nedellec, S.; Hulin, P.; Grégoire, M.; Blanquart, C.; Ishow, E. Hybrid Azo-fluorophore Organic Nanoparticles as Emissive Turn-on Probes for Cellular Endocytosis. *ACS Appl. Mater. Int.* **2019**, *11*, 32808-32814.

(25) Irie, M.; Fukaminato, T.; Sasaki, T.; Tamai, N.; Kawai, T. A digital fluorescent molecular photoswitch. *Nature* **2002**, *420*, 759.

(26) Naren, G.; Hsu, C. W.; Li, S. M.; Morimoto, M.; Tang, S. C.; Hernando, J.; Guirado, G.; Irie, M.; Raymo, F. M.; Sunden, H. et al. An All-Photonic Full Color RGB System Based On Molecular Photoswitches. *Nat. Commun.* **2019**, *10*, 3996.

(27) Roubinet, B.; Weber, M.; Shojaei, H.; Bates, M.; Bossi, M. L.; Belov, V. N.; Irie, M.; Hell, S. W. Fluorescent Photoswitchable Diarylethenes for Biolabeling and Single-Molecule Localization Microscopies with Optical Superresolution. *J. Am. Chem. Soc.* **2017**, *139*, 6611-6620.

(28) Nevskyi, O.; Sysoiev, D.; Oppermann, A.; Huhn, T.; Woll, D. Nanoscopic Visualization of Soft Matter Using Fluorescent Diarylethene Photoswitches. *Angew. Chem. Int. Ed.* **2016**, *55*, 12698-12702.

(29) Kim, D.; Jeong, K.; Kwon, J. E.; Park, H.; Lee, S.; Kim, S.; Park, S. Y. Dual-Color Fluorescent Nanoparticles Showing Perfect Color-Specific Photoswitching for Bioimaging and Super-Resolution Microscopy. *Nat. Commun.* **2019**, *10*, 3089.

(30) Kuo, C. T.; Thompson, A. M.; Gallina, M. E.; Ye, F. M.; Johnson, E. S.; Sun, W.; Yu, J. B.; Wu, I. C.; Fujimoto, B.; DuFort, C. C. et al. Optical painting and fluorescence activated sorting of single adherent cells labelled with photoswitchable Pdots. *Nat. Commun.* **2016**, *7*, 11468.

(31) Boucard, J.; Boudjemaa, R.; Steenkeste, K.; Jacqueline, C.; Stephant, N.; Lefevre, F. X.; Laurent, A. D.; Lartigue, L.; Hulin, P.; Nedellec, S. et al. Phosphonic Acid Fluorescent Organic Nanoparticles for High-Contrast and Selective Staining of Gram-Positive Bacteria. *ACS Omega* **2018**, *3*, 17392-17402.

(32) Sasaki, S.; Watanabe, T.; Ishibashi, Y.; Fukaminato, T.; Asahi, T. Giant Fluorescence Modulation Induced by UV-vis Excitation of Benzothiadiazole Nanoparticles Doped with Diarylethene Derivatives. *Chem. Lett.* **2018**, *47*, 163-166.

(33) Kundu, S.; Sk, B.; Pallavi, P.; Giri, A.; Patra, A. Molecular Engineering Approaches Towards All-Organic White Light Emitting Materials. *Chem. Eur. J.* **2020**, *26*, 5557-5582.

(34) Wilbraham, L.; Louis, M.; Alberga, D.; Brosseau, A.; Guillot, R.; Ito, F.; Labat, F.; Métivier, R.; Allain, C.; Ciofini, I. Revealing the Origins of Mechanically Induced Fluorescence Changes in Organic Molecular Crystals. *Adv. Mater.* **2018**, *30*, 1800817.

(35) *Photophysics of Molecular Materials: From Single Molecules to Single Crystals*; Lanzani G., Ed.; Wiley-VCH: Weinheim, 2006.

(36) Pandey, K. K.; Joshi, H. C.; Pant, T. C. Migration Effects on Excitation-Energy Transfer by Decay Analysis Using A Nanosecond Fluorimeter. *Chem. Phys. Lett.* **1988**, *148*, 472-478.

(37) Gosele, U.; Hauser, M.; Klein, U. K. A.; Frey, R. Diffusion and Long-Range Energy-Transfer. *Chem. Phys. Lett.* **1975**, *34*, 519-522.

(38) Ishibashi, Y.; Nakai, S.; Masuda, K.; Kitagawa, D.; Kobatake, S.; Asahi, T. Nanosecond Laser Photothermal Effect-Triggered Amplification of Photochromic Reactions in Diarylethene Nanoparticles. *Chem. Commun.* **2020**, *56*, 7088-7091.

(39) Su, J.; Fukaminato, T.; Placial, J. P.; Onodera, T.; Suzuki, R.; Oikawa, H.; Brosseau, A.; Brisset, F.; Pansu, R.; Nakatani, K. et al. Giant Amplification of Photoswitching by a Few

Photons in Fluorescent Photochromic Organic Nanoparticles. *Angew. Chem. Int. Ed.* **2016**, *55*, 3662-3666.

(40) Zhu, L.; Wu, W.; Zhu, M.-Q.; Han, J. J.; Hurst, J. K.; Li, A. D. Q. Reversibly Photoswitchable Dual-Color Fluorescent Nanoparticles as New Tools for Live-Cell Imaging. *J. Am. Chem. Soc.* **2007**, *129*, 3524-3526.

(41) Shimizu, K.; Métivier, R.; Kobatake, S. Synthesis and Fluorescence On/Off Switching of Hyperbranched Polymers Having Diarylethene at The Branching Point. *J. Photochem. Photobiol. A* **2020**, *390*, 112341.

(42) Yu, J. B.; Rong, Y.; Kuo, C. T.; Zhou, X. H.; Chiu, D. T. Recent Advances in the Development of Highly Luminescent Semiconducting Polymer Dots and Nanoparticles for Biological Imaging and Medicine. *Anal. Chem.* **2017**, *89*, 42-56.

(43) Schill, J.; Ferrazzano, L.; Tolomelli, A.; Schenning, A.; Brunsveld, L. Fluorene Benzothiadiazole Co-Oligomer Based Aqueous Self-Assembled Nanoparticles. *RSC Adv.* **2020**, *10*, 444-450.

TABLE OF CONTENTS / ABSTRACT GRAPHICS